Carbon 129 (2018) 750–757

Contents lists available at ScienceDirect

Carbon

journal homepage: www.elsevier.com/locate/carbon

Probing the formation of halogenated endohedral metallofullerenes: Predictions confirmed by experiments

Antonio Moreno-Vicente [a], Marc Mulet-Gas [b], Paul W. Dunk [b, ***], Josep M. Poblet [a, **], Antonio Rodríguez-Fortea [a, *]

[a] Departament de Química Física i Inorgànica, Universitat Rovira i Virgili, c/Marcel·lí Domingo 1, 43007, Tarragona, Spain
[b] National High Magnetic Field Laboratory, Florida State University, 1800 East Paul Dirac Drive, Tallahassee, FL 32310, USA

ARTICLE INFO

Article history:
Received 4 August 2017
Received in revised form
26 October 2017
Accepted 15 December 2017
Available online 21 December 2017

Dedicated to the memory of Prof. Harold W. Kroto.

ABSTRACT

The functionalization of endohedral metallofullerenes by halogenation has not been previously reported and remains a challenging endeavor in carbon nanoscience. In this work, we show that halogenation of endohedral metallofullerenes is predicted to be feasible based on thermodynamic grounds by means of DFT computations, combined with *in situ* experimental investigations. Computed bond energies for the chlorination, fluorination and hydrogenation of endohedral metallofullerenes that span a range of cage sizes are found to be comparable to those of known halogenated and hydrogenated empty fullerenes. Therefore, we propose that new forms of functionalized metallofullerenes should be synthesized under appropriate experimental conditions, despite many prior unsuccessful attempts. Indeed, we experimentally show for the first time that $M@C_{2n}$ (M = metal) metallofullerenes and the prototypical $Sc_3N@C_{80}$ clusterfullerene can be fluorinated by two different routes under the typical 'harsh' gas phase conditions of metallofullerene plasma synthesis, and at lower extents that could avoid cage degradation. The combination of halogenation and metal encapsulation offers the potential to create new radical-quenched, functionalized endohedral metallofullerenes that possess stable, large-gap carbon cages. These results open new avenues for the synthesis and stabilization of encapsulated molecular nanocarbons.

1. Introduction

Endohedral metallofullerenes (EMFs), i.e. fullerenes that contain metal atoms or metal-based clusters in the nanoscale space of their inner void [1,2], have been intensively studied over the last decade [3–6] because of their exceptional properties and potential applications in biomedicine and photovoltaics [7,8]. In general, exohedral functionalization is required to fully exploit these unique compounds. For example, water-soluble gadofullerenols are used as powerful contrast agents [9]. Besides, the external groups might impart complementary features to EMFs that tune their physical properties for use as acceptors in polymer solar cells [7] or as donor-acceptor dyad conjugates [10,11]. Cycloaddition reactions as well as radical additions are among the most used methods to obtain EMF-monoadducts [1,12,13]. Poly-perfluoroalkylated EMFs, for example, $Sc_3N@C_{80}(CF_3)_n$ (n = 2-16), have been synthesized by means of high temperature reaction schemes. However, direct fluorination was not successful for this prototypical nitride EMF despite attempts under many experimental conditions [14], a behavior that is completely unlike that of hollow fullerenes. Here, we show based on DFT computations that halogenation (fluorination and chlorination), as well as hydrogenation of EMFs, which has remained underexplored so far, are predicted to be favored derivatizations based on thermodynamic considerations. Further, we theoretically and experimentally investigate several forms of fluorinated and hydrogenated small, non-IPR monometallic endofullerenes, as well as examine fluorination of pristine $Sc_3N@C_{80}$, a medium-sized clusterfullerene, at low levels of addition. Our results provide fundamental chemical insight into the halogenation of metallofullerenes and show that optimization of synthetic conditions to achieve low poly-addition levels can lead to new halogenated EMFs, which could also be further functionalized in a

* Corresponding author.
** Corresponding author.
*** Corresponding author.
E-mail addresses: dunk@magnet.fsu.edu (P.W. Dunk), josepmaria.poblet@urv.cat (J.M. Poblet), antonio.rodriguezf@urv.cat (A. Rodríguez-Fortea).

https://doi.org/10.1016/j.carbon.2017.12.056
0008-6223/

rather easy and selective manner [15,16].

Two primary routes are known to stabilize fullerenes that do not satisfy the isolated pentagon rule (i.e., non-IPR fullerenes): (i) endohedral encapsulation or (ii) exohedral halogenation or hydrogenation. The first isolated and characterized non-IPR fullerene, $Sc_2@C_{66}$, was stabilized by encapsulation of two Sc atoms [17]. Although the cage was initially assigned to be isomer $C_{2v}(4348)$-C_{66}, which contains two pairs of pentagon adjacencies (pentalene motifs), it was not until 2014 that an X-ray crystal structure was solved and the cage was found to be $C_{2v}(4059)$-C_{66}, a thermodynamically favored isomer predicted by computations and exhibits two triply sequentially fused pentagon motifs (TSFP2), as shown in Fig. 1 [18]. However, empty cage C_{66} has been recently characterized as deca-chlorinated, $C_{2v}(4348)$-$C_{66}Cl_{10}$ (Fig. 1) [19]. Numerous examples of endohedral or halogenated non-IPR fullerenes are known today, demonstrating the intensive interest in efforts to stabilize non-IPR carbon cages [1,20]. Different factors govern encapsulation and halogenation of fullerenes. Encapsulation is mainly explained by charge transfer from the internal metal atom or cluster to the cage [21–24], whereas halogenation is directed largely by the strain released upon exohedral functionalization, as well as the aromaticity of the remaining planar substructures in the cage and the steric hindrance between the halogens [25,26]. In addition, kinetic stability is gained once encapsulation or halogenation takes place due to a significant increase of the molecular HOMO-LUMO gap [22,25]. Thus, it is of high interest to determine if the combination of these two factors might lead to halogenated EMFs, which could exhibit new fullerene cages and/or facilitate functionalization. Besides, it is a promising route to obtain stable radical-quenched EMFs with large gap, as for example $La@C_{82}$-X, $M@C_{66}$-X or $Sc_3O@C_{80}$-X [27,28].

2. Experimental

2.1. Gas-phase synthesis of fluorinated EMFs from doped graphite starting material

Composite rods that are comprised of graphite (99.9999%), $SrCO_3$ (99.9%), and polytetrafluoroethylene (99.9%) are thoroughly mixed and then molded into a composite rod by compression. $Sr@C_{50}F_n$ and $C_{50}F_n$ are formed *in situ* by use of a pulsed supersonic cluster source by a single laser pulse of a Nd:YAG laser (532 nm, 5-10 mj/pulse) under a flow of helium. The gas-phase reaction products were analyzed by a custom-built 9.4 T FT-ICR mass spectrometer directly coupled to the cluster source and are conducted with positive ions [29]. Ions produced by 10 individual vaporization events were accumulated and transferred by octopoles to an open cylindrical trap. The ions are then accelerated to a detectable radius by a broadband frequency sweep excitation, and detected as the differential current induced between two opposed electrodes of the ICR cell. The positively charged molecular ions are expected to be representative of the neutral abundance distribution generated by laser vaporization. Although, we note that the corresponding neutrals may exhibit different stabilities.

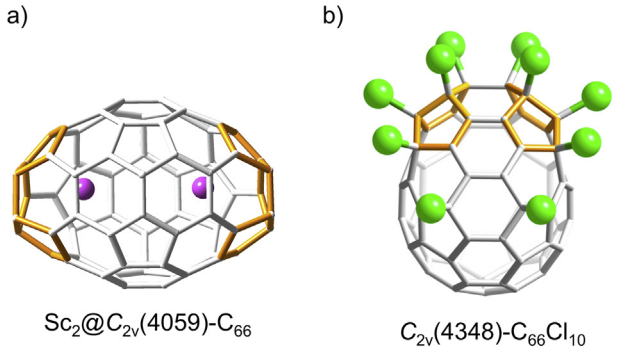

Fig. 1. Structures of two C_{66} fullerenes stabilized by endohedral or exohedral modification: a) the dimetallic endohedral fullerene $Sc_2@C_{2v}(4059)$-C_{66} with two triply sequentially fused pentagon motifs (TSFP2) and b) the deca-chlorinated $C_{2v}(4348)$-$C_{66}Cl_{10}$ with two adjacent pentagon pairs (APP2). Pentagon adjacencies are highlighted in orange, C in grey, Cl in green and Sc in magenta. (A colour version of this figure can be viewed online.)

2.2. Fluorination of pristine $Sc_3N@C_{80}$ by exposure to F-containing carbon vapor

Macroscopic samples of the pure metallic nitride clusterfullerene $Sc_3N@C_{80}$ is uniformly applied to the surface of a PTFE-doped graphite target rod (25% PTFE). Upon laser vaporization, pre-existing $Sc_3N@C_{80}$ is primarily desorbed into the gas phase, after which it interacts with F-containing plasma generated from the solid PTFE-doped graphite to achieve *in situ* fluorination. All experiments are conducted with positive ions.

2.3. CID experiments

Halogenated reaction products (positive ions) are isolated in the ICR cell by a stored waveform inverse Fourier transform (SWIFT) excitation and then thermally excited, through collisions with helium, in an ultra-high vacuum by sustained off resonance irradiation collision-induced dissociation (SORI-CID) [29]. Externally halogenated products are confirmed by F loss with retention of the pristine cage and encapsulated metals or clusters.

2.4. Computational details

The geometry optimizations were performed at density functional theory (DFT) level with the ADF 2013.01 program [30,31]. The exchange-correlation functionals of Becke and Perdew (BP86) and the Slater TZP basis sets were used (BP86/TZP level) [32,33]. Frozen cores consisting of (i) the 1s shell for C, N, O and F; (ii) the 1s to 2p shells for S, Ca and Sc; (iii) the 1s to 3d shells for Sr and Y; (iv) the 1s to 4d shells for La were used. Relativistic corrections were included by means of the ZORA formalism. In addition, the Grimme Dispersion D3 method was considered [34].

Car-Parrinello molecular dynamics simulations were carried out using CPMD program [35,36]. The description of the electronic structure was based on the expansion of the valence electronic wave functions into a plane wave basis set, which was limited by an energy cutoff of 90 Ry. The interaction between the valence electrons and the ionic cores was treated through the pseudopotential (PP) approximation (Martins-Troullier type) [37]. The functional by Perdew, Burke and Ernzerhoff (PBE) was selected as density functional [38]. We used a fictitious electron mass of 900 a.u. The simulations were carried out using periodic boundary conditions in a cubic cell with a side length of 17 Å and a time step of 0.144 fs. Dispersion corrections were also included. Car-Parrinello MD simulations were done at 873 K, a temperature that is slightly higher than those applied in the fluorination of $Sc_3N@I_h$-C_{80} when using a wide variety of fluorinating agents [14].

Our criteria to select the EMF-X_q regioisomers is the following: 1) For non-IPR cages, we have functionalized those sites in the pentalene bonds or near them (atoms with rather high pyramidalization angles) because they possess higher BDEs; 2) For the C_{60}, C_{70} and C_{80} IPR cages, we based our choice on retainment of the highest possible symmetry. For example, C_{60}-X exhibits a single isomer because all sixty carbons are equivalent by symmetry. For

C_{60}-X_2, the number of possible isomers increases dramatically, and therefore, we constrained functionalization to the 6-6 and 5-6 bonds, and other regioisomers in which the two X atoms are far apart, i.e. 1,4 position in a hexagon; 3) For the IPR La@C_{82}, which is a radical, we based our choice on the spin density of the C atoms.

3. Results and discussion

3.1. Endohedral monometallofullerenes

Computed fullerene–X bond energies (X = Cl, F, H) reveal chemical insight into reactivity of the different carbon atoms that comprise a given fullerene. Bond energies in the pentalene motifs are significantly higher than in other C atoms with lower pyramidalization angles. Therefore, the more planar and aromatic regions of the cage are less reactive (see Table S1 and Fig. S1 for some chlorinated empty cages). To assess the feasibility of halogenation or hydrogenation for various forms of EMFs, we have computed at BP86/TZP level (see Computational Details) fullerene–X bond dissociation energies for some of their most stable isomers. Bond dissociation energies (BDE) are defined as BDE = E ($C_{2n}X_q$) – E (C_{2n}) – qE(X). Firstly, we have considered M@C_{2n}, where M = Ca, Sr and 2n = 50 and 60, which are the most abundant cages, i.e. magic-numbered species, found for divalent monometallic endofullerenes [29]. In particular, we have computed the BDE for the lowest-energy isomers in each family, namely M@D_{5h}(271)-C_{50} and M@I_h-C_{60} [29]. In addition, we have also considered cage C_{2v}(1809)-C_{60}, with two adjacent pentagon pairs (APP2), since M@C_{2v}(1809)-C_{60} shows an energy that is slightly above that of M@I_h-C_{60} (13 kcal mol^{-1} at BP86/TZP level) and it has been found to be chlorinated as empty cage [39]. Finally, we have computed the BDEs for the prototypical radical La@C_{2v}(9)-C_{82}. We would like to emphasize here that it is not our goal to perform an exhaustive study of all the possible *q* halogenation positions within each of these cages to find the lowest-energy possible regioisomer $C_{2n}X_q$ nor to understand the addition sequences [25,26,40], but to show that halogenation and hydrogenation are feasible processes for any of these cages if appropriate experimental conditions did exist (see Computational Details for the criteria used to select the computed regioisomers).

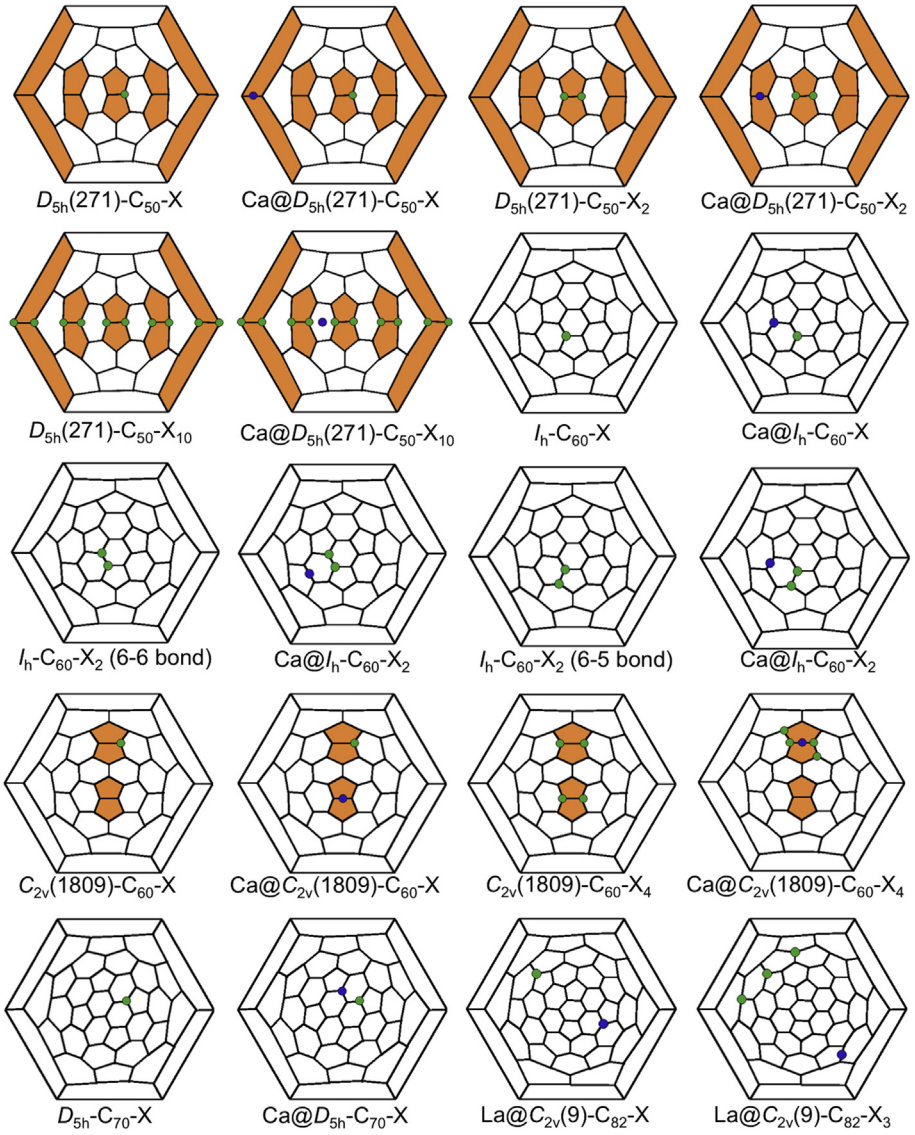

Fig. 2. Schlegel diagrams for the fullerenes analyzed in Table 1. Green balls show the position of X atoms; blue balls show the position of the cage where the internal M atom is pointing to; pentagon adjacencies are highlighted in orange. (A colour version of this figure can be viewed online.)

As general trends (Table 1 and S2-S3 and Fig. 2), we find that (i) C atoms with low pyramidalization angles show lower BDEs compared to C atoms in pentalene motifs, which are much more strained. Thus, release of strain is a key factor for halogenation of metallofullerenes; (ii) BDEs for fluorinated and hydrogenated fullerenes are much larger than for chlorinated cages, in agreement with the strength of the C–X (X = F, H or Cl) bonds; (iii) Although there is no a clear trend in BDEs upon inclusion of the metal atom, in general, they are not considerably modified (less than 15%); and (iv) the nature of the (divalent) metal does not significantly affect the BDEs. We note that, in contrast to other cages (trend iii), the BDEs for M@I_h-C_{60}-X are substantially increased compared to empty I_h-C_{60}-X. That observation is attributed to result from the open-shell (bi-radicaloid) character for the M@I_h-C_{60} system, which becomes significantly stabilized upon addition of F, Cl or H atoms; on the other hand, empty I_h-C_{60} is already very stable without halogen addition. For I_h-C_{60}-X_2, we found a different effect of the metal depending on the regioisomer; while bis-adduct on the 6-6 bond does not appreciably change the BDEs upon M encapsulation, bis-adduct on the 5-6 bond significantly does (Table 1). Inspection of the frontier molecular orbital energies in the empty I_h-C_{60}-X_2 shows that 5-6 bis-adducts have low-energy LUMO orbitals, thus explaining their higher stability compared to 6-6 bis-adducts once the divalent metal (Ca or Sr) is encapsulated. On the other hand, insertion of the metal does not noticeably change the BDEs for the non-IPR C_{2v}(1809)-C_{60} cage, regardless the addition level (q = 1 or 4). And for additions on the smaller non-IPR D_{5h} (271)-C_{50}, encapsulation slightly reduces the BDEs from around 5% for q = 10 up to 10-14% for q = 2. Finally, BDEs for halogenation and hydrogenation of the prototypical radical La@C_{2v}(9)-C_{82} to yield closed-shell functionalized EMFs (q = 1 and 3) are comparable to those of smaller C_{60} and C_{50} cages.

Further, we find that there is nearly identical behavior of the bond dissociation (or formation) free energies for empty fullerenes, which have been already detected and isolated, and endofullerenes when varying temperature (see Fig. S11). Therefore, we predict halogenation or hydrogenation of monometallic endofullerenes to be a favorable process, especially for non-IPR cages such as D_{5h} (271)-C_{50} (Table 1 and Fig. 3), which show BDEs similar to those of reported empty cage analogues, D_{5h} (271)-C_{50}-Cl_{10} [41,42]. IPR monometallic endofullerenes as M@I_h-C_{60}-X_q (q = 1, 2) are also likely to be observed. In addition, we found that recombination of X atoms on the surface of the fullerene to yield X_2 is not thermodynamically favored (see Table S5). However, why empty fullerenes are found to be halogenated or hydrogenated and endofullerenes have not been observed as such so far?

We have examined *in situ* halogenation for these species by use of a pulsed laser vaporization cluster source, analyzed by ultrahigh resolution Fourier transform ion cyclotron resonance (FT-ICR) mass spectrometry to experimentally corroborate our theoretical predictions. Fig. 4 and Fig. S5 unambiguously show that mono- and di-fluorinated small empty cages (e.g., C_{50}), as well as the mono-fluorinated endofullerenes, Sr@C_{50} and Sr@C_{60}, form after vaporization of Sr- and polytetrafluoroethylene (PTFE)-doped graphite starting material (5% Sr, 2% PTFE) in the presence of He buffer gas. C_{50} and Sr@C_{50}, for example, are generated directly from the bulk starting material, and thereafter, halogenation reactions occur in the gas phase upon interaction with atomic F. Under the present conditions, the extent of fluorination is primarily due to the low quantity of F available for reaction with the carbon cages. Further, the endofullerene, Sr@C_{50}, is present in lower relative abundance compared to C_{50} and thus its mono-fluorinated product is formed in inherently lower abundance. Identification of fluorinated cages are further confirmed by collision-induced dissociation (CID) experiments, performed by means of sustained off-resonance irradiation techniques (Fig. S6) [29]. Thus, halogenated mono-metallofullerenes may have not been previously observed due to low production yield compared to empty cages.

In addition to fluorinated C_{50} and Sr@C_{50}, molecular ions are observed that correspond to other even-numbered fullerene cages, as well as cages that contain a carbon adatom (i.e., odd-numbered species) [43–45] and their fluorinated forms. We proposed that all carbon cages, including those with an adatom, are formed through a bottom-up formation mechanism, and thereafter, are fluorinated in the gas phase at a sufficiently lower temperature.

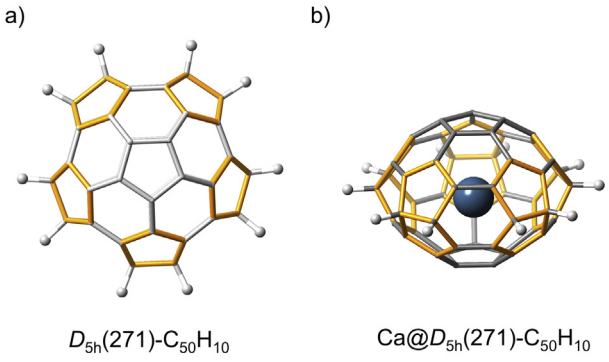

Fig. 3. Structures of a) the empty cage D_{5h} (271)-$C_{50}H_{10}$ with five adjacent pentagon pairs, view along the C_5 axis; and b) the monometallic endofullerene Ca@D_{5h} (271)-$C_{50}H_{10}$, view perpendicular to the C_5 axis. Pentagon adjacencies are highlighted in orange. C in grey, H in light grey and Ca in blue. (A colour version of this figure can be viewed online.)

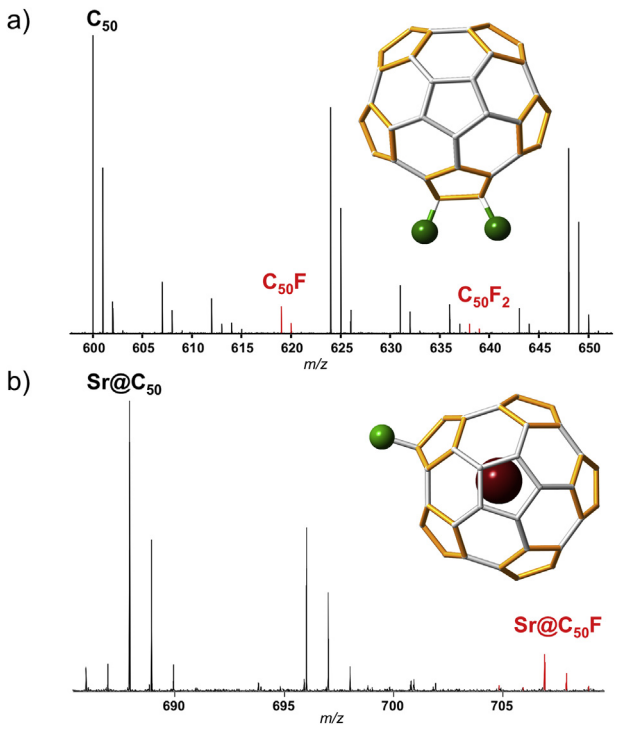

Fig. 4. FT-ICR mass spectra (positive ions) that show fluorinated products formed by laser vaporization of Sr- and F-containing graphite starting material: a) empty C_{50} cage, $C_{50}F$ and $C_{50}F_2$; and b) the mono-metallic endofullerene Sr@$C_{50}F$ (only mono-fluorination). In the inset, suggested structures for a) D_{5h} (271)-$C_{50}F_2$ and for b) Sr@D_{5h} (271)-$C_{50}F$. Pentagon adjacencies are highlighted in orange. C in grey, F in dark green and Sr in dark red. (A colour version of this figure can be viewed online.)

3.2. Endohedral clusterfullerenes

Clusterfullerenes, in general, possess larger cages than mono-metallic endofullerenes because clusters of atoms do not fit in small cages. For larger fullerenes, the number of possible IPR isomers increases (one for C_{60} and C_{70}, seven for C_{80}, 46 for C_{90}, 450 for C_{100}, etc.) and thus it is more likely to find an IPR cage suitable to encapsulate a cluster. Indeed, both IPR and non-IPR cages have been found to encapsulate metal clusters [1], in which $M_3N@C_s(51365)$-C_{84} (M = Tb, Tm and Gd) is the metallofullerene with the largest non-IPR cage characterized by X-ray diffraction so far [46,47]. The prototypical and most abundant EMF, $Sc_3N@I_h(7)$-C_{80} [48], as well as $Sc_3N@D_{5h}(6)$-C_{80}, which exhibit IPR cages, were trifluoromethylated few years ago, to form $Sc_3N@C_{80}(CF_3)_q$ (q = 2, 4, 6) [49]. In addition, higher levels of trifluoromethylation have been achieved recently (q = 14, 16, 18) [14,50]. Extensively hydrogenated $Sc_3N@I_h(7)$-$C_{80}H_{52}$ was predicted to be thermodynamically stable using DFT [51], but hydrogenation of $Sc_3N@I_h(7)$-C_{80} has not been observed to date. In 2011, Boltalina, Popov and co-workers reported that the halogenation behavior of $Sc_3N@C_{80}$ is very different from that of empty fullerenes. For example, synthetic methods that were successfully used to fluorinate empty fullerenes did not result in observable $Sc_3N@C_{80}F_q$ products [14]. In fact, fluorinated $Sc_3N@C_{80}$ has not been previously observed to the best of our knowledge, which may be due to cage degradation that occurs upon fluorination under particular conditions [14]. Car-Parrinello MD simulations corroborate this idea (*vide infra*).

We computed the EMF–X BDEs (X = Cl, F and H) for several representative nitride, sulfide and oxide clusterfullerenes as well as di-metallic endofullerenes and compare them with some empty cages (Table 2 and S4 and Fig. 5) to gain insight into the change in C-X bond strength upon encapsulation. Analogous general trends as for mono-metallic endofullerenes are observed (see above). Principally, release of strain is found again to be the main factor for halogenation of clusterfullerenes. As shown in Table 2 and S4, BDEs to C atoms with higher pyramidalization angles, as in pentalene bonds in non-IPR cages, are significantly larger than BDEs to those C atoms with lower degrees of pyramidalization, as those in IPR cages or in hexagon-hexagon-pentagon junctions in non-IPR cages. We also find that changing the internal cluster, when the charge transferred and the size (approximately) are conserved, does not significantly affect the BDEs. Halogenation and hydrogenation of $Sc_2@C_{2v}(4059)$-C_{66} are highly favorable processes and exhibit BDE (and free-energy) values similar to the already observed $C_{2v}(4348)$-C_{66}–Cl_{10} as well as to those of smaller, more strained cages (compare Tables 1 and 2 and Figs. S2–S4 and S7–S10). Low extents of halogenation in $Y_3N@C_s(39663)$-C_{82} (q = 2) are also particularly favored (Table 2). Additions to IPR $Sc_3N@I_h(7)$-C_{80}, albeit which shows lower BDEs than for non-IPR structures, are still very favorable in a thermodynamic sense.

We have experimentally probed the gas-phase halogenation of pre-existing $Sc_3N@I_h(7)$-C_{80} by means of the laser-based technique [29,52,53]. As shown in Fig. 6, we find that $Sc_3N@I_h(7)$-$C_{80}F_q$ (q = 1 and 2) species are readily formed after exposure of the pristine clusterfullerene precursor to fluorine-doped carbon plasma, achieved by vaporization of a $Sc_3N@C_{80}$-coated PTFE-doped graphite target (25% PTFE). Upon laser vaporization, $Sc_3N@C_{80}$ is primarily desorbed into the gas phase, and thereafter, carbon insertion reactions take place that form $Sc_3N@C_{82}$ and larger Sc_3N encapsulated cages [53]. We propose that fluorination of these carbon species

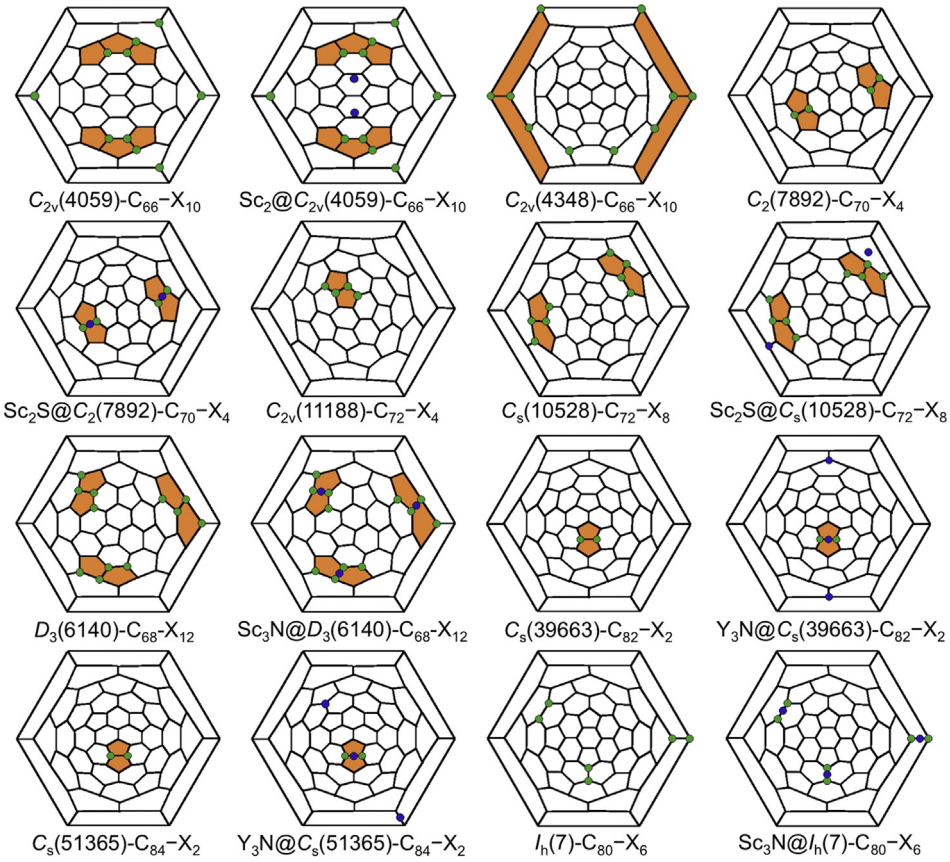

Fig. 5. Schlegel diagrams for the fullerenes analyzed in Table 2. Green balls show the position of X atoms; blue balls show the position of the cage where the internal M atom is pointing to; pentagon adjacencies are highlighted in orange. (A colour version of this figure can be viewed online.)

Table 1
Bond dissociation energies (BDE) for halogenated and hydrogenated fullerenes and endohedral mono-metallofullerenes.[a,b]

Fullerene	Cage	X = Cl	X = F	X = H
D_{5h} (271)-C_{50}–X	APP5	54.7	89.9	77.7
Ca@D_{5h} (271)-C_{50}–X	APP5	44.3	79.8	65.6
Sr@D_{5h} (271)-C_{50}–X	APP5	43.0	79.9	63.8
D_{5h} (271)-C_{50}–X_2	APP5	58.1	94.7	81.7
Ca@D_{5h} (271)-C_{50}–X_2	APP5	49.4	86.6	71.1
Sr@D_{5h} (271)-C_{50}–X_2	APP5	48.6	85.6	70.6
D_{5h} (271)-C_{50}–X_{10}	APP5	56.8	93.5	80.1
Ca@D_{5h} (271)-C_{50}–X_{10}	APP5	53.0	89.9	75.3
Sr@D_{5h} (271)-C_{50}–X_{10}	APP5	53.1	90.0	75.6
I_h-C_{60}–X	IPR	30.7	65.4	51.1
Ca@I_h-C_{60}–X	IPR	49.7	86.0	66.8
Sr@I_h-C_{60}–X	IPR	49.8	86.0	66.8
I_h-C_{60}–X_2 (6-6 bond)	IPR	40.6	78.4	66.3
Ca@I_h-C_{60}–X_2	IPR	40.2	77.9	66.8
Sr@I_h-C_{60}–X_2	IPR	40.8	78.7	67.2
I_h-C_{60}–X_2 (5-6 bond)	IPR	34.2	70.3	58.9
Ca@I_h-C_{60}–X_2	IPR	47.9	85.8	68.4
Sr@I_h-C_{60}–X_2	IPR	47.6	85.6	68.1
C_{2v}(1809)-C_{60}–X	APP2	45.3	80.2	67.2
Ca@C_{2v}(1809)-C_{60}–X	APP2	43.8	78.7	65.8
Sr@C_{2v}(1809)-C_{60}–X	APP2	43.6	79.0	65.7
C_{2v}(1809)-C_{60}–X_4	APP2	49.6	86.2	71.5
Ca@C_{2v}(1809)-C_{60}–X_4	APP2	48.2	86.0	70.4
Sr@C_{2v}(1809)-C_{60}–X_4	APP2	47.7	85.4	70.7
D_{5h}-C_{70}–X	IPR	29.2	63.5	49.6
Ca@D_{5h}-C_{70}–X	IPR	48.6	84.9	64.7
Sr@D_{5h}-C_{70}–X	IPR	45.7	82.4	61.9
La@C_{2v}(9)-C_{82}–X	IPR	42.7	77.6	63.2
La@C_{2v}(9)-C_{82}–X_3	IPR	44.6	79.3	65.9

[a] Energies in kcal mol^{-1} per added X = H, F or Cl atom.
[b] Structures for computed fullerenes are shown in Fig. 2 and S2-S4.

takes place at lower temperature and after carbon insertion reactions. Dissociation investigations by means of SORI-CID unambiguously demonstrate that $Sc_3N@C_{80}F$ and the other fluorinated products are exohedrally modified clusterfullerenes (Fig. S13). Other fluorinated clusterfullerene molecular ions are observed that correspond to $Sc_3N@C_{82}F$, whereby the parent $Sc_3N@C_{82}$ species form through bottom-up growth of $Sc_3N@C_{80}$ [53]. Therefore, fluorination of endohedral fullerenes in the gas phase may also be used as a method to further characterize formation mechanisms.

Low levels of addition do not significantly distort the C_{80} cage structure, and therefore, prevents cage degradation that is a major

Table 2
Bond dissociation energies (BDE) for halogenated and hydrogenated fullerenes and clusterfullerenes.[a,b]

Fullerene	Cage	X = Cl	X = F	X = H
C_{2v}(4059)-C_{66}–X_{10}	TSFP2	52.1	93.2	74.9
$Sc_2@C_{2v}$(4059)-C_{66}–X_{10}	TSFP2	53.3	88.4	72.2
C_{2v}(4348)-C_{66}–X_{10}	APP2	51.4	88.6	74.6
C_2 (7892)-C_{70}–X_4	APP2	54.0	90.3	76.1
$Sc_2S@C_2$ (7892)-C_{70}–X_4	APP2	42.3	79.1	63.6
C_{2v}(11188)-C_{72}–X_4	APP1	51.6	87.8	72.8
C_s(10528)-C_{72}–X_8	APP2	49.3	86.5	72.4
$Sc_2S@C_s$(10528)-C_{72}–X_8	APP2	43.6	81.0	65.5
$Sc_2O@C_s$(10528)-C_{72}–X_8	APP2	44.9	82.2	66.6
D_3 (6140)-$C_{68}X_{12}$	APP3	47.6	84.4	69.7
$Sc_3N@D_3$ (6140)-C_{68}–X_{12}	APP3	43.1	80.6	65.2
C_s(39663)-C_{82}–X_2	APP1	49.4	85.6	70.7
$Y_3N@C_s$(39663)-C_{82}–X_2	APP1	46.3	83.7	65.7
C_s(51365)-C_{84}–X_2	APP1	47.7	88.2	72.8
$Y_3N@C_s$(51365)-C_{84}–X_2	APP1	42.6	79.6	63.0
I_h(7)-C_{80}–X_6	IPR	36.9	74.2	62.8
$Sc_3N@I_h$(7)-C_{80}–X_6	IPR	27.8	63.7	50.3

[a] Energies in kcal mol^{-1} per added X = H, F or Cl atom.
[b] Structures for computed fullerenes are shown in Fig. 5 and Figs. S7–S9.

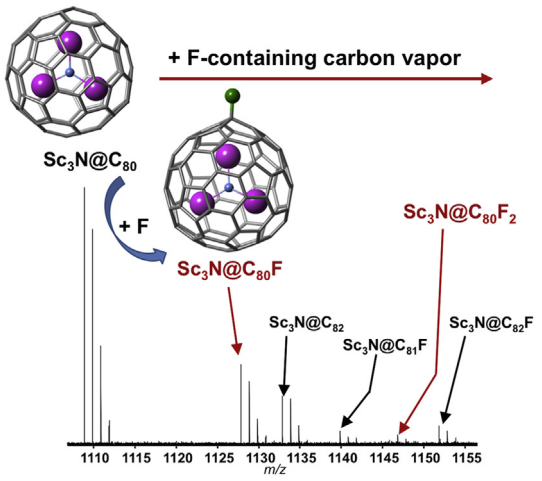

Fig. 6. Cluster cations formed after pristine $Sc_3N@C_{80}$ is exposed to fluorine-containing carbon vapor, generated from polytetrafluoroethylene-doped graphite. The mono-fluorinated cation, $Sc_3N@C_{80}$-F, is the dominant formation product. The larger species, such as $Sc_3N@C_{82}F$, form by the growth of $Sc_3N@C_{80}$ and subsequent fluorination. (A colour version of this figure can be viewed online.)

obstacle for synthesis of these derivatives. Car-Parrinello MD simulations performed under similar conditions compared to those of experimental fluorination (see Computational Details) show that highly fluorinated systems, such as $Sc_3N@I_h(7)$-$C_{80}F_q$ (q = 44 and 72), suffer extensive distortions of the cage compared to $Sc_3N@I_h(7)$-$C_{80}F_6$ (Fig. S14), even at the short time scale simulated here (20 ps). Indeed, for $Sc_3N@I_h(7)$-$C_{80}F_{72}$, we observed the opening of the cage at only 5 ps and its subsequent degradation in less than 10 ps (see Fig. 7). Even though we did not observe the breakage of the cage for $Sc_3N@I_h(7)$-$C_{80}F_{44}$ in the 20-ps trajectory, we found that many of its C-C bonds appreciably elongate to distances of 1.9–2.0 Å (see Fig. S14). Therefore, we conclude that optimized synthetic conditions to achieve low levels of addition would be necessary to halogenate or hydrogenate clusterfullerenes. We would like to emphasize here that the observed IPR $Sc_3N@I_h(7)$-$C_{80}F$ shows lower BDEs than any of the non-IPR clusterfullerenes in Table 2. The 'cage breakage' that we show in Fig. 7 is not related to the formation of the mono- and di-fluorinated species in this work, but rather to distinguish how low level fluorinated endofullerenes may be more stable than very highly fluorinated species. Further, we expect that other forms of endofullerenes may be fluorinated by the methods reported in this work.

4. Conclusions

By means of computations and online chemical sampling of

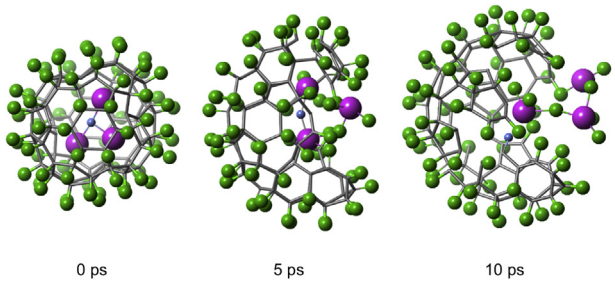

Fig. 7. Snapshots of the Car-Parrinello MD trajectory of $Sc_3N@I_h(7)$-$C_{80}F_{72}$ at experimental conditions of fluorination (t = 0, 5 and 10 ps) where it is shown clearly the degradation suffered by the carbon cage at high levels of F addition, in contrast to lower extents of halogenation. (A colour version of this figure can be viewed online.)

pulsed laser vaporization synthesis analyzed by ultrahigh resolution FT-ICR mass spectrometry, we have reported for the direct halogenation of endohedral metallofullerenes. Computed bond dissociation energies (BDEs) performed at the DFT level for chlorination, fluorination and hydrogenation of a range of cage sizes and isomers lead to two significant conclusions: (i) metal encapsulation may change BDEs compared to empty cages, albeit to a low extent (e.g., up to 15%); and (ii) the effect of the internal metal or cluster does not appreciably modify (within 5%) BDEs, provided that the charge transferred and the approximate size are conserved. We have found that, according to computed bond energies and free energies, IPR and non-IPR endohedral monometallic or clusterfullerenes may be halogenated or hydrogenated under appropriate synthetic conditions. Indeed, we have shown that Sr@C_{50}, Sr@C_{60} and the prototypical Sc_3N@I_h-C_{80} metallofullerenes can be fluorinated, and at lower extents that may avoid cage degradation, through two experimental routes under the typical *in situ* gas-phase conditions of metallofullerene plasma synthesis. These functionalizations are shown to stabilize small metallofullerenes and might render these nanoforms isolable or detectable from arc-discharge produced soot. Further, the halogenated clusterfullerenes may hold the potential to act as precursors to facilitate formation of species with alternative functionalizations. Endohedral metal encapsulation combined with exohedral halogenation of fullerene cages may be a useful approach to successfully form new radical-quenched, large-gap metallofullerenes, and should be applicable to the synthesis and stabilization of other encapsulated molecular nanocarbons.

Acknowledgments

This work was supported by the Spanish Ministerio de Ciencia e Innovación (Project No. CTQ2014-52774-P) and by the Generalitat de Catalunya (2014SGR-199 and XRQTC). J.M.P. thanks the ICREA foundation for an ICREA ACADEMIA award. A portion of this work was performed at the National High Magnetic Field Laboratory, which is supported by the NSF Cooperative Agreement through DMR-11-57490 and the State of Florida.

Appendix A. Supplementary data

Supplementary data related to this article includes lists of binding energies for all the mono EMFs and clusterfullerenes computed, their Schlegel representations as well as detailed information about the experiments and can be found at https://doi.org/10.1016/j.carbon.2017.12.056.

A data set colletion of computational results is available in the ioChem-BD repository [54] and can be accessed via https://doi.org/10.19061/iochem-bd-2-15.

References

[1] A.A. Popov, S.F. Yang, L. Dunsch, Endohedral fullerenes, Chem. Rev. 113 (2013) 5989–6113.
[2] A. Rodriguez-Fortea, A.L. Balch, J.M. Poblet, Endohedral metallofullerenes: a unique host-guest association, Chem. Soc. Rev. 40 (2011) 3551–3563.
[3] M.N. Chaur, F. Melin, A.L. Ortiz, L. Echegoyen, Chemical, electrochemical, and structural properties of endohedral metallofullerenes, Angew. Chem. Int. Ed. 48 (2009) 7514–7538.
[4] C.H. Chen, L. Abella, M.R. Ceron, M.A. Guerrero-Ayala, A. Rodriguez-Fortea, M.M. Olmstead, X.B. Powers, A.L. Balch, J.M. Poblet, L. Echegoyen, Zigzag Sc_2C_2 carbide cluster inside a 88 fullerene cage with one heptagon, Sc_2C_2@C_s(hept)-C_{88}: a kinetically trapped fullerene formed by C-2 insertion? J. Am. Chem. Soc. 138 (2016) 13030–13037.
[5] X. Lu, L. Bao, T. Akasaka, S. Nagase, Recent progress in the chemistry of endohedral metallofullerenes, Chem. Commun. 50 (2014) 14701–14715.
[6] T. Wang, C. Wang, Endohedral metallofullerenes based on spherical I_h-C_{80} cage: molecular structures and paramagnetic properties, Acc. Chem. Res. 47 (2014) 450–458.
[7] R.B. Ross, C.M. Cardona, D.M. Guldi, S.G. Sankaranarayanan, M.O. Reese, N. Kopidakis, J. Peet, B. Walker, G.C. Bazan, E. Van Keuren, B.C. Holloway, M. Drees, Endohedral fullerenes for organic photovoltaic devices, Nat. Mater. 8 (2009) 208–212.
[8] C. Shu, F.D. Corwin, J. Zhang, Z. Chen, J.E. Reid, M. Sun, W. Xu, J.H. Sim, C. Wang, P.P. Fatouros, A.R. Esker, H.W. Gibson, H.C. Dorn, Facile preparation of a new gadofullerene-based magnetic resonance imaging contrast agent with high ^{1}H relaxivity, Bioconjugate Chem. 20 (2009) 1186–1193.
[9] J.F. Zhang, P.P. Fatouros, C.Y. Shu, J. Reid, L.S. Owens, T. Cai, H.W. Gibson, G.L. Long, F.D. Corwin, Z.J. Chen, H.C. Dorn, High relaxivity trimetallic nitride (Gd_3N) metallofullerene MRI contrast agents with optimized functionality, Bioconjugate Chem. 21 (2010) 610–615.
[10] J.R. Pinzon, C.M. Cardona, M. Angeles Herranz, M.E. Plonska-Brzezinska, A. Palkar, A.J. Athans, N. Martin, A. Rodriguez-Fortea, J.M. Poblet, G. Bottari, T. Torres, S.S. Gayathri, D.M. Guldi, L. Echegoyen, Metal nitride cluster fullerene M_3N@C_{80} (M = Y, Sc) based dyads: synthesis, and electrochemical, theoretical and photophysical studies, Chem. Eur J. 15 (2009) 864–877.
[11] J.R. Pinzon, M.E. Plonska-Brzezinska, C.M. Cardona, A.J. Athans, S.S. Gayathri, D.M. Guldi, M.A. Herranz, N. Martin, T. Torres, L. Echegoyen, Sc_3N@C_{80}-ferrocene electron-donor/acceptor conjugates as promising materials for photovoltaic applications, Angew. Chem. Int. Ed. 47 (2008) 4173–4176.
[12] X. Lu, L. Feng, T. Akasaka, S. Nagase, Current status and future developments of endohedral metallofullerenes, Chem. Soc. Rev. 41 (2012) 7723–7760.
[13] S. Osuna, M. Swart, M. Sola, The reactivity of endohedral fullerenes. What can be learnt from computational studies? Phys. Chem. Chem. Phys. 13 (2011) 3585–3603.
[14] N.B. Shustova, D.V. Peryshkov, I.V. Kuvychko, Y.S. Chen, M.A. Mackey, C.E. Coumbe, D.T. Heaps, B.S. Confait, T. Heine, J.P. Phillips, S. Stevenson, L. Dunsch, A.A. Popov, S.H. Strauss, O.V. Boltalina, Poly(perfluoroalkylation) of metallic nitride fullerenes reveals addition-pattern guidelines: synthesis and characterization of a family of Sc_3N@$C_{80}(CF_3)_n$ (n=2-16) and their radical anions, J. Am. Chem. Soc. 133 (2011) 2672–2690.
[15] E.A. Khakina, A.A. Yurkova, A.S. Peregudov, S.I. Troyanov, V.V. Trush, A.I. Vovk, A.V. Mumyatov, V.M. Martynenko, J. Balzarini, P.A. Troshin, Highly selective reactions of $C_{60}Cl_6$ with thiols for the synthesis of functionalized 60 fullerene derivatives, Chem. Commun. 48 (2012) 7158–7160.
[16] A.B. Kornev, E.A. Khakina, S.I. Troyanov, A.A. Kushch, A. Peregudov, A. Vasilchenko, D.G. Deryabin, V.M. Martynenko, P.A. Troshin, Facile preparation of amine and amino acid adducts of 60 fullerene using chlorofullerene $C_{60}Cl_6$ as a precursor, Chem. Commun. 48 (2012) 5461–5463.
[17] C.R. Wang, T. Kai, T. Tomiyama, T. Yoshida, Y. Kobayashi, E. Nishibori, M. Takata, M. Sakata, H. Shinohara, Materials science - C_{66} fullerene encaging a scandium dimer, Nature 408 (2000) 426–427.
[18] M. Yamada, H. Kurihara, M. Suzuki, J.D. Guo, M. Waelchli, M.M. Olmstead, A.L. Balch, S. Nagase, Y. Maeda, T. Hasegawa, X. Lu, T. Akasaka, Sc_2@C_{66} revisited: an endohedral fullerene with scandium ions nestled within two unsaturated linear triquinanes, J. Am. Chem. Soc. 136 (2014) 7611–7614.
[19] C.L. Gao, X. Li, Y.Z. Tan, X.Z. Wu, Q. Zhang, S.Y. Xie, R.B. Huang, Synthesis of long-sought C_{66} with exohedral stabilization, Angew. Chem. Int. Ed. 53 (2014) 7853–7855.
[20] Y.Z. Tan, S.Y. Xie, R.B. Huang, L.S. Zheng, The stabilization of fused-pentagon fullerene molecules, Nature Chem. 1 (2009) 450–460.
[21] J. Aihara, Kinetic stability of carbon cages in non-classical metallofullerenes, Chem. Phys. Lett. 343 (2001) 465–469.
[22] A.A. Popov, L. Dunsch, Structure, stability, and cluster-cage interactions in nitride clusterfullerenes M_3N@C_{2n} (M = Sc, Y; 2n=68-98): a density functional theory study, J. Am. Chem. Soc. 129 (2007) 11835–11849.
[23] A. Rodriguez-Fortea, N. Alegret, A.L. Balch, J.M. Poblet, The maximum pentagon separation rule provides a guideline for the structures of endohedral metallofullerenes, Nature Chem. 2 (2010) 955–961.
[24] H. Shinohara, Endohedral metallofullerenes, Rep. Prog. Phys. 63 (2000) 843–892.
[25] C.L. Gao, L. Abella, Y.Z. Tan, X.Z. Wu, A. Rodriguez-Fortea, J.M. Poblet, S.Y. Xie, R.B. Huang, L.S. Zheng, Capturing the fused-pentagon C_{74} by stepwise chlorination, Inorg. Chem. 55 (2016) 6861–6865.
[26] Y. Wang, S. Diaz-Tendero, M. Alcami, F. Martin, Relative stability of empty exohedral fullerenes: pi delocalization versus strain and steric hindrance, J. Am. Chem. Soc. 139 (2017) 1609–1617.
[27] L. Abella, Q.Q. Tang, X.X. Zhang, Y.F. Wang, N. Chen, J.M. Poblet, A. Rodriguez-Fortea, Sc_3O@$I_h(7)$-C_{80}: a trimetallic oxide clusterfullerene abundant in the raw soot, J. Phys. Chem. C 120 (2016) 26159–26167.
[28] D. Xu, Z. Wang, H. Shinohara, Capturing the unconventional metallofullerene M@C_{66} by trifluoromethylation: a theoretical study, ChemPhysChem 18 (2017) 3007–3011.
[29] P.W. Dunk, M. Mulet-Gas, Y. Nakanishi, N.K. Kaiser, A. Rodriguez-Fortea, H. Shinohara, J.M. Poblet, A.G. Marshall, H.W. Kroto, Bottom-up formation of endohedral mono-metallofullerenes is directed by charge transfer, Nat. Commun. 5 (2014) 5844.
[30] E.J. Baerends, D.E. Ellis, P. Ros, ADF, Department of Theoretical Chemistry, Vrije Universiteit, Amsterdam, 2013.
[31] G.T. te Velde, F.M. Bickelhaupt, E.J. Baerends, C.F. Guerra, S.J.A. Van Gisbergen, J.G. Snijders, T. Ziegler, Chemistry with ADF, J. Comput. Chem. 22 (2001) 931–967.
[32] A.D. Becke, DEnsity functional calculations of molecular-bond energies, J. Chem. Phys. 84 (1986) 4524–4529.

[33] J.P. Perdew, Density-functional approximation for the correlation-energy of the inhomogeneous electron-gas, Phys. Rev. B 33 (1986) 8822–8824.
[34] S. Grimme, S. Ehrlich, L. Goerigk, Effect of the damping function in dispersion corrected density functional theory, J. Comput. Chem. 32 (2011) 1456–1465.
[35] CPMD, Copyright IBM Corp 1990-2015, 1997–2001. Copyright MPI für Festkörperforschung Stuttgart, http://www.cpmd.org.
[36] R. Car, M. Parrinello, Unified approach for molecular dynamics and density-functional theory, Phys. Rev. Lett. 55 (1985) 2471–2474.
[37] N. Troullier, J.L. Martins, Efficient pseudopotentials for plane-wave calculations, Phys. Rev. B 43 (1991) 1993–2006.
[38] J.P. Perdew, K. Burke, M. Ernzerhof, Generalized gradient approximation made simple, Phys. Rev. Lett. 77 (1996) 3865–3868.
[39] Y.-Z. Tan, Z.-J. Liao, Z.-Z. Qian, R.-T. Chen, X. Wu, H. Liang, X. Han, F. Zhu, S.-J. Zhou, Z. Zheng, X. Lu, S.-Y. Xie, R.-B. Huang, L.-S. Zheng, Two I_h-symmetry-breaking C_{60} isomers stabilized by chlorination, Nat. Mater. 7 (2008) 790–794.
[40] A. Vlandas, C.P. Ewels, G. Van Lier, Controlling fullerene addition sequences, regioselectivity and magic numbers via metal encapsulation, Chem. Commun. 47 (2011) 7051–7053.
[41] J.H. Chen, Z.Y. Gao, Q.H. Weng, W.S. Jiang, Q. He, H. Liang, L.L. Deng, S.L. Xie, H.Y. Huang, X. Lu, S.Y. Xie, K. Shi, R.B. Huang, L.S. Zheng, Combustion synthesis and electrochemical properties of the small hydrofullerene $C_{50}H_{10}$, Chem. Eur J. 18 (2012) 3408–3415.
[42] S.Y. Xie, F. Gao, X. Lu, R.B. Huang, C.R. Wang, X. Zhang, M.L. Liu, S.L. Deng, L.S. Zheng, Capturing the labile fullerene 50 as $C_{50}Cl_{10}$, Science 304 (2004), 699–699.
[43] J.F. Christian, Z.M. Wan, S.L. Anderson, C_{61}^{+} Production and decomposition in $^{13}C^{+} + C_{60}$ collisions: C-atom exchange and the fragmentation-pattern as a function of energy, J. Phys. Chem. 96 (1992) 3574–3576.
[44] P.W. Dunk, N.K. Kaiser, C.L. Hendrickson, J.P. Quinn, C.P. Ewels, Y. Nakanishi, Y. Sasaki, H. Shinohara, A.G. Marshall, H.W. Kroto, Closed network growth of fullerenes, Nat. Commun. 3 (2012).
[45] C.P. Ewels, M.I. Heggie, P.R. Briddon, Adatoms and nanoengineering of carbon, Chem. Phys. Lett. 351 (2002) 178–182.
[46] C.M. Beavers, T.M. Zuo, J.C. Duchamp, K. Harich, H.C. Dorn, M.M. Olmstead, A.L. Balch, $Tb_3N@C_{84}$: an improbable, egg-shaped endohedral fullerene that violates the isolated pentagon rule, J. Am. Chem. Soc. 128 (2006) 11352–11353.
[47] T. Zuo, K. Walker, M.M. Olmstead, F. Melin, B.C. Holloway, L. Echegoyen, H.C. Dorn, M.N. Chaur, C.J. Chancellor, C.M. Beavers, A.L. Balch, A.J. Athans, New egg-shaped fullerenes: non-isolated pentagon structures of $Tm_3N@C_s(51365)$-C_{84} and $Gd_3N@C_s(51365)$-C_{84}, Chem. Commun. (2008) 1067–1069.
[48] S. Stevenson, G. Rice, T. Glass, K. Harich, F. Cromer, M.R. Jordan, J. Craft, E. Hadju, R. Bible, M.M. Olmstead, K. Maitra, A.J. Fisher, A.L. Balch, H.C. Dorn, Small-bandgap endohedral metallofullerenes in high yield and purity, Nature 401 (1999) 55–57.
[49] N.B. Shustova, A.A. Popov, M.A. Mackey, C.E. Coumbe, J.P. Phillips, S. Stevenson, S.H. Strauss, O.V. Boltalina, Radical trifluoromethylation of $Sc_3N@C_{80}$, J. Am. Chem. Soc. 129 (2007), 11676-+.
[50] S.F. Yang, C.B. Chen, M.Z. Jiao, N.B. Tamm, M.A. Lanskikh, E. Kemnitz, S.I. Troyanov, Synthesis, isolation, and addition patterns of trifluoromethylated D_{5h} and I_h isomers of $Sc_3N@C_{80}$: $Sc_3N@D_{5h}$-$C_{80}(CF_3)_{18}$ and $Sc_3N@I_h$-$C_{80}(CF_3)_{14}$, Inorg. Chem. 50 (2011) 3766–3771.
[51] J.M. Campanera, M.I. Heggie, R. Taylor, Analysis of polyaddition levels in i-Sc_3NC_{80}, J. Phys. Chem. B 109 (2005) 4024–4031.
[52] M.A. Duncan, Invited review article: laser vaporization cluster sources, Rev. Sci. Instrum. 83 (2012).
[53] M. Mulet-Gas, L. Abella, M.R. Ceron, E. Castro, A.G. Marshall, A. Rodriguez-Fortea, L. Echegoyen, J.M. Poblet, P.W. Dunk, Transformation of doped graphite into cluster-encapsulated fullerene cages, Nat. Commun. 8 (2017) 1222.
[54] M. Alvarez-Moreno, C. de Graaf, N. Lopez, F. Maseras, J.M. Poblet, C. Bo, Managing the computational chemistry big data problem: the iochem-BD platform, J. Chem. Inf. Model. 55 (2015) 95–103.